Article

Robust Static Structural System Identification Using Rotations

Jun Lei [1,2], José Antonio Lozano-Galant [3] , Dong Xu [4], Feng-Liang Zhang [2,*] and Jose Turmo [5]

1. Key Laboratory of Earthquake Engineering and Engineering Vibration, Institute of Engineering Mechanics, China Earthquake Administration, Harbin 150086, China; donovan_lj@163.com
2. School of Civil and Environmental Engineering, Harbin Institute of Technology, Shenzhen 518055, China
3. Department of Civil Engineering, University of Castilla-La Mancha, 13071 Ciudad Real, Spain; JoseAntonio.Lozano@uclm.es
4. Department of Bridge Engineering, Tongji University, Shanghai 200092, China; xu_dong@tongji.edu.cn
5. Department of Civil and Environmental Engineering, Universitat Politècnica de Catalunya, BarcelonaTech, 08034 Barcelona, Spain; jose.turmo@upc.edu
* Correspondence: zhangfengliang@hit.edu.cn

Abstract: Deflections are commonly measured in the static structural system identification of structures. Comparatively less attention has been paid to the possibility of measuring rotations for structural system identification purposes, despite the many advantages of using inclinometers, such as a high resolution and being reference free. Although some work using rotations can be found in the literature, this paper, for the very first time, proposes a statistical analysis that justifies the theoretical advantage of measuring rotations. The analytical expressions for the target parameters are obtained via static structural system identification using the constrained observability method first. Combined with the inverse distribution theory, the probability density function of the estimations of the target parameters can be obtained. Comparative studies on a simply supported bridge and a frame structure demonstrate the advantage of measuring rotations regarding the unbiasedness and the extent of variation in the estimations. To achieve robust parameter estimations, four strategies to use redundant rotations are proposed and compared. Numerical verifications on a bridge structure and a high-rise building have shown promising results.

Keywords: rotations; static; observability; structural system identification; inverse distribution

1. Introduction

1.1. Existing Structural System Identification Method

Potential catastrophic events due to the failure or malfunction of civil infrastructures (e.g., bridges, high-rise buildings, dams) might claim people's lives and cause substantial economic losses. To avoid this undesirable consequence, it is vital to know the current condition of structures. For this reason, structural health monitoring (SHM) and structural system identification have attracted much attention in recent decades [1–3]. A basic assumption in structural system identification is that the deterioration or the damage of structures is reflected in the change in structural parameters (such as bending and axial stiffness). These parameters can be estimated by various structural system identification methods using a measured response from structures under external excitations.

Dynamic-based methods account for the majority of structural system identification methods. Depending on the source of excitation, dynamic structural system identification methods are categorized as input–output methods and output-only methods. In the input–output methods, the time history of the excitation and the response are measured to compute frequency response functions. These functions are used to determine the natural frequencies, mode shapes, and damping ratios of the structure using well-established methods [4–6]. In the output-only methods [7,8], instead of using heavy, cumbersome and expensive devices to excite large-scale structures in a controlled way, the ambient (wind-induced, traffic-induced and subtle seismic) vibrations are measured conveniently

and economically. The modal information of structures can be obtained by analyzing the correlation functions or the spectral density matrices computed from the operating response data. Among these methods, the Bayesian methods [8] can obtain the posterior distributions of the target parameters by combining the assumed distributions of the parameters in the priors and the evidence from the measurements. The error-domain model [9–11] can identify parameter values in the existence of systematic errors and detect the presence of unrecognized systematic errors. The residual minimization method [12] can localize model errors and estimate physical parameters by minimizing the force unbalance in the equations of motion.

Compared with dynamic methods, static structural system identification methods are much less developed. Sanayei et al. [13] identified the plate-bending stiffness of a reinforced concrete pier deck with incomplete static test data using accurate forces and displacements. Later, Banan et al. [14] formulated structural system identification as a constrained nonlinear least squares problem by minimizing the discrepancies between the measured and predicted displacements or forces. Hjelmstad et al. [15] incorporated an adaptive parameter grouping strategy with the work from Banan. The proposed method can locate and assess damage even under sparse and noisy measurements. Yang et al. [16] were able to locate and quantify damages in a cantilever beam and two trusses using a flexibility disassembly technique with a baseline model and all DOFs measured. Sun et al. [17] approximated the beam curvatures by the second-order difference of deflections. This work was able to locate damage from the abnormality in the curvature curves while the damage extent could not be quantified.

Recently, observability methods [18,19] were applied in the field of state estimation. This method was able to identify whether a set of available measurements was sufficient to estimate the state of systems. Lozano et al. [20] applied the observability method (OM) to determine the observability of structural parameters in 2D beam models symbolically with static measurements. Later, structural system identification by numerical OM (NOM) was proposed by Nogal [21] to carry out numerical estimation of target parameters. Recently, Tomás et al. [22] and Emadi et al. [23] developed this method to deal with actual measurements on site, including shear deformations. The effects of measurement errors and simulation errors on the estimation accuracy were investigated in [24]. Later, Lei [25] derived the analytical relations that the displacements of beam-like structure should satisfy using OM. The adverse effect of measurement errors on the estimation accuracy was reduced by imposing the compatibility conditions. A new formulation of observability equation with the measurement error terms separated was proposed in [26].

1.2. Application of Inclinometers in Civil Engineering

Existing static structural system identification methods largely measure deflections rather than rotations [16,17,27]. However, wide industrial applications (e.g., automotive, electronics and aviation industries) of inclinometers can be found [28]. The merits of inclinometers make them very desirable for SHM applications [29–33]. Application of inclinometers in SHM of civil structures can be found in the literature; for instance, stadiums Design Plaza Building [34], Tianjin 117 (597 m) [35], construction hoists [36], Lutrive Bridge [32], pavement construction [37], ground movement [38] and slope measurement [39]. In particular, inclinometers are used to reconstruct the deflected shape of bridges due to the difficulty in measuring deflections directly. However, direct use of rotations might be preferred because systematic errors might be introduced into the approximated deflections depending on the assumption made in the basic functions (e.g., precalculated deflected shapes [32], polynomials [40]). Zhang estimated the deflections accurately via the partial least squares method from a Finite Element Model (FEM) without using basis functions [33]. The possibility of locating damage using inclinometers was also investigated in this work. Liu [37] achieved real-time measurement of lift-thickness during highway construction using a system-integrating inclinometer, robotic total station, and laser ranging sensors. Ha et al. [38] developed and applied a wireless MEMS-based

borehole inclinometer for automated measurement of ground movement. Hou [41] proposed to monitor interstory drift in building structures via rotation measurements with MEMS inclinometers and an optimized sensor layout. A comparison of inclinometers versus deflection measurements has already been investigated using information entropy metrics [42]. Different metrics to evaluate the goodness of sensor placement were also studied by Papadimitriou [43] and Argyris [44].

1.3. Research Objective

The novelty of this method is that it can determine the observability of target parameters when a measurement set is given. It is highlighted that a systematic procedure to carry out statistical analysis of the distribution of parameter θ using analytical expression is presented. The expression for parameter θ is obtained under the framework of static structural system identification using the observability method. The distribution of the parameters can be determined by the analytical expression from OM and the theory of inverse distribution [45]. The advantage of this method is that it can obtain analytical expression of the target parameters which have clear physical meaning and mathematical elegance. It can avoid the heavy computation burden that normally occurs in the Bayesian method or optimization-based method.

Although inclinometers have been used in SHM for a long time, the research on the use of rotations in structural system identification is very limited. In the case of static structural system identification for beam-like structures [25], it is found that the estimations of bending stiffness were more sensitive to the measurement errors in deflections than errors in rotations using Monte Carlo analysis. However, no theoretical advantage of using rotations can be found. A comparative study of the use of rotations and/or deflections was carried out to justify the theoretical advantage of using rotations over deflections regarding the unbiasedness and the extent of variation in the estimations. Different strategies to use redundant rotations with the aim of improving estimation accuracy are also discussed.

The remainder of this paper is organized as follows. Section 2 describes the algorithm for structural system identification by constrained OM [46], which obtains the analytical expressions for the parameters. Then, the procedure to carry out statistical analysis with the resulting expression is also presented in this section. Section 3 adopts two illustrative examples to justify the theoretical advantages of using rotations over deflections. Section 4 investigates the effectiveness of four strategies to make use of redundant rotations in a high-rise building. Finally, some conclusions are presented in Section 5.

2. Methodology

This section presents the methodology to carry out statistical distribution of the estimations. In Section 2.1, structural system identification using the Constrained Observability Method is introduced. Then, the procedure to carry out the statistical analysis of the distribution of estimations is described in Section 2.2.

2.1. Structural System Identification Using the Constrained Observability Method

In a previous study [20], the observability of structural parameters was determined symbolically by checking the null space of the coefficient matrix of a system of equations adapted from equilibrium equations. The null space for a $m \times n$ matrix $[A]$ is the vector space whose vectors satisfy the homogeneous equation as shown in Equation (1).

$$[A]\{x\} = \{0\} \tag{1}$$

The null space for matrix $[A]$ is defined in Equation (2).

$$Null([A]) = \{\{x\} \in R^n | [A]\{x\} = 0\} \tag{2}$$

The null space matrix $[N]$ for the matrix $[A]$ is a matrix whose columns form a basis of the null space $Null([A])$, which can be computed by Gaussian elimination. In fact,

any vector in the null space is a linear combination of the basis vectors for *Null*([*A*]), i.e., columns of the matrix [*N*]. In structural system identification using both OM and NOM, the identification of structural parameters is a recursive process in which the parameters that are identified in the last recursive step are incorporated into the input of the current recursive step to enable the identification of other parameters. In each recursive step, the nonlinear variables appearing in the system of equations are treated as linearized ones. However, the assumption of linearity might reduce the number of observable parameters with given measurement sets [39]. Then, two-stage structural system identification using the constrained OM (COM) was proposed. In Stage 1, the original structural system identification using NOM is carried out until no more parameters are observable. In Stage 2, the system of equations from the last recursive step in Stage 1 is reformulated as a constrained optimization problem, minimizing the square sum of the residuals of this system. The procedure to carry out structural system identification using COM is described in the seven steps below, and all the seven steps are the novelty of this method. Stage 1 is related to Steps 2–5, while Stage 2 is related to Step 7.

Step 1: Define an initial FEM using 2D beam elements for the structure to be analyzed. Generate the system of equilibrium equations for this FEM, as shown by Equation (3).

$$[K]\{\delta\} = \{f\} \tag{3}$$

The matrix [*K*] is the global stiffness matrix that includes the information of length L_j, elastic moduli E_j, area A_j and inertia I_j of element j ($j = 1, 2 \ldots N_e$). The displacement vector $\{\delta\}$ comprises horizontal deflection u_i, vertical deflection v_i and rotation w_i of node i ($i = 1, 2 \ldots N_n$). The force vector $\{f\}$ comprises horizontal force H_i, vertical force V_i and moment M_i applied on node i ($i = 1, 2 \ldots N_n$). The numbers of elements and nodes in the FEM are denoted by N_e and N_n.

Step 2: Introduce the boundary conditions and values of the increments in displacements and forces during the static test to obtain the observability equations.

The entries in the matrix [*K*] are sums of monomial ratios, which are the ratios between axial or bending stiffnesses and the square (or cubic) of the length, i.e., $\frac{E_j A_j}{L_j}$, $\frac{E_j I_j}{L_j^2}$ or $\frac{E_j I_j}{L_j^3}$. In static structural system identification, it is assumed that L_j is known and E_j, A_j and I_j are unknown parameters to be estimated. Note that E_j, A_j, I_j and L_j from different elements might appear in the same entry due to element connectivity. To separate these parameters, each column of matrix [*K*] is divided into multiple columns such that any resulting column is uniquely related to one monomial (stiffness), $E_j A_j$ or $E_j I_j$. Meanwhile, the displacement vector $\{\delta\}$ is expanded correspondingly. Then, these stiffnesses are extracted from the matrix [*K*] and the expanded displacement vector is multiplied by them. Hence, a (constant) modified matrix $[K^*]$ and a modified vector $\{\delta^*\}$ composed of nonlinear products, e.g., $E_j A_j u_i$, $E_j I_j w_i$, $E_j I_j v_i$, are obtained, as shown in Equation (4).

$$[K^*] \cdot \{\delta^*\} = \{f\} \tag{4}$$

Once the boundary conditions and the forces applied in the non-destructive static test have been defined, it is assumed that a subset of increments in deflections $\{\delta_1^*\}$ of $\{\delta^*\}$ are known and a subset of forces $\{f_1\}$ are known, while the remaining parts $\{\delta_0^*\}$ and $\{f_0\}$ are unknown. By static condensation, Equation (4) can be partitioned as Equation (5).

$$[K^*]\{\delta^*\} = \begin{bmatrix} K_{00}^* & K_{01}^* \\ K_{10}^* & K_{11}^* \end{bmatrix} \begin{Bmatrix} \delta_0^* \\ \delta_1^* \end{Bmatrix} = \begin{Bmatrix} f_0 \\ f_1 \end{Bmatrix} = \{f\} \tag{5}$$

To cluster the unknowns $\{\delta_0^*\}$ and $\{f_0\}$, Equation (5) can be rewritten equivalently as the observability equation, Equation (6). I and 0 are the null and the identity matrices.

$$[B]\{z\} = \begin{bmatrix} K_{10}^* & 0 \\ K_{00}^* & -I \end{bmatrix} \begin{Bmatrix} \delta_0^* \\ f_0 \end{Bmatrix} = \begin{Bmatrix} f_1 - K_{11}^* \delta_1^* \\ -K_{01}^* \delta_1^* \end{Bmatrix} = \{D\} \tag{6}$$

Step 3: Check the null space matrix $[N]$ of the coefficient matrix $[B]$ to determine the observability of unknowns in $\{z\}$ and obtain the numerical estimations for observable variables. The structure of the general solution $\{z_g\}$ to Equation (6) is given by Equation (7).

$$\{z_g\} = \{z_p\} + \{z_h\} = \begin{Bmatrix} \delta_0^* \\ f_0 \end{Bmatrix}_p + [N] \cdot \{\rho\} \tag{7}$$

$\{z_p\}$ is a particular solution to Equation (6) and $\{z_h\}$ is a solution to the homogeneous version of Equation (6) (i.e., the vector $[D]$ is replaced by zeros). $\{z_h\}$ is a linear combination of the columns of the matrix $[N]$. The coefficients of the linear combination are denoted by the vector $\{\rho\}$. The observability of unknowns in the vector $\{z\}$ is determined by checking null rows in the matrix $[N]$. If any row in the matrix $[N]$ is null, then the same row of $\{z_h\}$ is also null. Then, the associated variable in $\{z_g\}$ is determined by the particular solution $\{z_p\}$. Hence, the variable is uniquely determined and observable. The calculation of the null space matrix $[N]$ should be carried out symbolically to avoid omitting observable variables, because close-to-zero values from numerical calculations might appear in those null rows. The numerical values of the observable variables are obtained from the particular solution of Equation (6) using least squares methods.

Step 4: Check whether new variables in the unknown vector $\{z\}$ were identified or not. If identified, go to Step 5. Otherwise, go to Step 6.

Step 5: Any identified variables will be incorporated into the preceding input to form the subsequent input and initiate a new recursive step. This may enable the identification of other unknowns in $\{z\}$. Steps 2–4 are repeated until no more variables can be identified.

Step 6: Check whether all variables are identified or not. If all the parameters are identified, then end the procedure. Otherwise, go to Step 7.

Step 7: Obtain the estimations of parameters by solving the constrained optimization problem that is adapted from the observability equations in the last recursive step. Since the linearization of the unknowns leads to the reduction in observable unknowns, the nonlinearity in structural system identification is regained by means of solving an optimization problem with the constraints that the linearized products are equal to the product of associated single variables, e.g., $EI_2v_2 = EI_2 \cdot v_2$.

Some single variables $\{z_s\}$ may not appear in the unknown vector $\{z\}$ of Equation (6). A new unknown vector $\{z^*\}$ is obtained by adding $\{z_s\}$ in $\{z\}$. A null matrix $[\Omega]$ is introduced into the coefficient matrix so that the equations are not violated, as shown in Equation (8).

$$[B^*] \cdot \{z^*\} = [B \ \Omega] \begin{Bmatrix} z \\ z_s \end{Bmatrix} = \{D\} \tag{8}$$

The objective function (Equation (9)) of the optimization is to minimize the square sum of the residuals (unbalanced nodal forces) in Equation (8).

$$f(\{z^*\}) = \sum_{i=1}^{3N_n} \epsilon_i^2 \tag{9}$$

where ϵ_i is the residual of the *ith* equation in Equation (8), and N_n is the number of nodes.

The procedure to carry out structural system identification by COM is summarized in Figure 1.
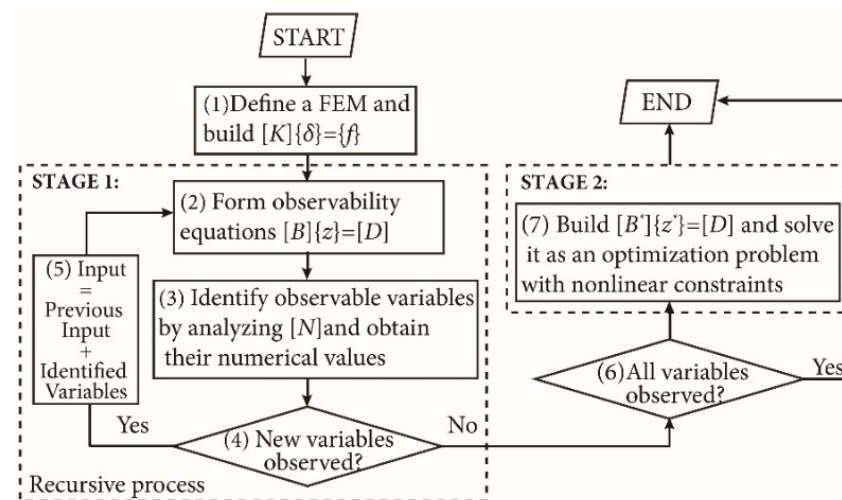
Figure 1. Flowchart of the algorithm for structural system identification by COM.

In stage 1 (Steps 2–5), the observability equations are treated linearly such that the computation is much reduced when compared with nonlinear methods. All the steps in stage 1 are the same as those in structural system identification by NOM. In stage 2 (Step 7), nonlinearity is introduced by imposing constraints via optimization, with the aim of identifying more parameters. As some parameters have been identified in stage 1, the solution space for the optimization algorithm to explore in stage 2 is much reduced, which eases the computation and convergence issues.

It is highlighted that the observability of the parameters can be analyzed in the 7-step procedure. The observability analysis can differentiate the meaningful estimations from those estimations obtained using numerical optimization. That is to say, the numerical estimations from optimization can always provide numerical values for all parameters, but some values are not meaningful as they are not observable due to the limited number or the limited spatial distribution of measurements.

2.2. Procedure for the Statistical Analysis of the Distribution of Estimations

In Step 3 (Figure 1) of the structural system identification using COM described in Section 2.1, instead of obtaining numerical estimations of the variables, the analytical expressions can be obtained symbolically using Gaussian elimination. The obtained analytical expression of the structural parameters is in the form of a fraction with the measurements in the denominator. In this paper, it is assumed that measurement errors follow a normal distribution. Random errors are added to theoretical displacements (usually generated by the FEM) in a proportional manner, as indicated by Equation (10).

$$\widetilde{\delta} = \delta_r \cdot (1 + E_{level} \cdot \xi) \tag{10}$$

where δ_r is the displacement obtained from FEM and E_{level} is the error level; ξ is a random number that follows a normal distribution with zero mean and standard deviation 0.5. The setting of this value is to be consistent with previous research. The effect of choosing such a value is the decrease in the dispersion of the distribution of errors. Hence, it reduces the chance of obtaining more extreme errors.

As the random variables are in the denominator, the definition of inverse distribution is introduced here. Let X be a random variable and the random variable Y be the inverse of X, i.e., $Y = 1/X$. Then, the distribution of Y is the inverse distribution of X. A closed-form solution for the probability density function (PDF) of the distribution of Y is available when the random variable X follows a normal distribution [45]. If the normally distributed

variable X has a mean of μ and standard deviation of σ, i.e., $X \sim N(\mu,\sigma^2)$, the PDF of the random variable $Y = 1/X$ (or the inverse distribution of X) is given by Equation (11).

$$p_Y(y|\mu,\sigma) = \frac{1}{\sqrt{2\pi}\sigma y^2} e^{-\frac{[(\frac{1}{y})-\mu]^2}{2\sigma^2}} \tag{11}$$

The distribution of Y is bimodal, and it has a negative mode at y_1 and a positive mode at y_2.

$$y_1 = -\frac{\mu + \sqrt{\mu^2 + 8\sigma^2}}{4\sigma^2}, \; y_2 = \frac{-\mu + \sqrt{\mu^2 + 8\sigma^2}}{4\sigma^2} \tag{12}$$

The mean and standard deviation for the distribution of Y at a specified interval can be calculated by associated integrations of the PDF p_Y. These formulas can be found in classic statistic books [45]. With Equations (11) and (12) and the analytical expression of the parameters, the procedure to carry out statistical analysis of the distribution of estimations can be summarized below, and is depicted in Figure 2. Illustrative examples are provided and discussed in detail in Section 3.
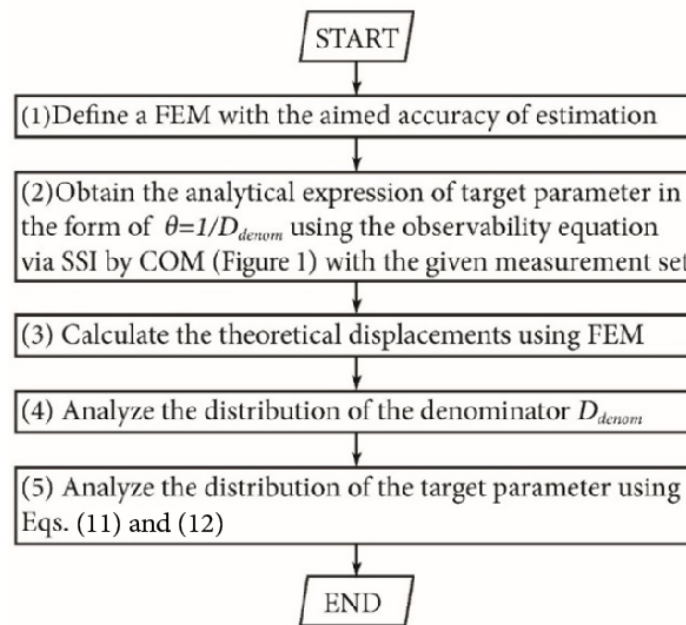

Figure 2. Procedure for the statistical analysis of target parameters.

Step 1: Define a FEM for the structure to be analyzed according to the targeted accuracy of estimations.
Step 2: Choose a measurement set to obtain the analytical expression for the target parameter θ, employing structural system identification using COM (see Section 2.1). Rewrite this expression for θ as the reciprocal of an expression denoted by D_{denom}, i.e., $\theta = 1/D_{denom}$.
Step 3: Calculate the theoretical displacements of the structure using the finite element method.
Step 4: Analyze the distribution of D_{denom} using Equation (10) and the theoretical values obtained in Step 3.
Step 5: Analyze the distribution of $\theta = 1/D_{denom}$ using Equations (11) and (12).

In the parameter estimation problem in power systems, if a measurement set of n measurements is able to identify all the n parameters and the drop in any measurement fails to do so, then this set is defined as an essential set [47]. The availability of analytical expressions for static structural system identification using COM depends on the number and the type of measurements in Step 2. When less than the required measurements, which is equal to the number of unknown parameters, are used, the target parameter is not observable [48]. Neither analytical expressions nor numerical estimations can be obtained.

When more than the required measurements are used, the target parameters are observable and can be numerically evaluated, while the analytical expressions are not obtainable. The necessary measurements can be determined by trial and error methods, i.e., adding one measurement each time until the analytical expressions are obtained. It is noted that the trial-and-error method can be carried out using computer programs. However, in the case of a large structure, it could be a heavy workload as there are many combinations of different DOFs. This trial-and-error method certainly can be helped by engineering judgement, which makes the workload much lighter. The measurement sets that are capable of deriving the analytical expressions for the target parameters θ are referred to as essential sets of parameters θ.

In the whole process, MATLAB was used to develop a code based on the procedure in Figures 1 and 2.

3. Theoretical Motivation for Measuring Rotations

The advantages of using rotations are not limited to the practical issues mentioned in Section 1.2. Statistical analyses of two structures were carried out to emphasize the theoretical motivation of measuring rotations rather than deflections. Example 1 corresponds to a simply supported bridge, while example 2 corresponds to a two-story frame.

3.1. Statistical Analysis of a Simply Supported Bridge

Example 1 was a simply supported bridge measuring 3*L* long. Statistical analysis was carried out for this structure using different measurement sets. The parameterization of the FEM for this structure is shown in Figure 3. The target parameter was EI_2. OM (observability method) indicates that any two rotations, or one rotation plus two deflections, or three deflections, in nodes 5–9 are qualified to identify EI_2. Without loss of generality, three measurement sets, set 1 (v_5, v_7, v_9), set 2 (v_5, v_7, w_9) and set 3 (w_5, w_9), were studied, where v_i and w_i denote the measured deflection and rotation, respectively.
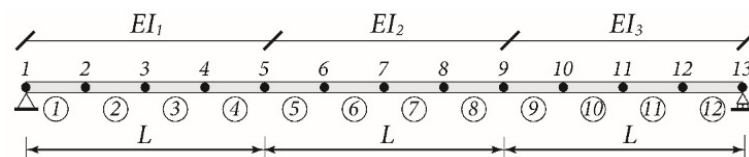

Figure 3. FEM for a simply supported bridge.

Employing structural system identification using COM with set 3 (w_5, w_9), the analytical expression of EI_2 (as shown in Equation (13)) can be obtained by solving the observability equation symbolically.

$$EI_2^{set3} = \frac{L}{32(w_5 - w_9)} \cdot \left\{ 16 \sum_{i=1}^{5} (M_i - M_{14-i}) + 8M_6 - 8M_8 + 4 \sum_{i=2}^{5} [(i-1)V_iL + (i-1)V_{14-i}L] + 19V_6L + 20V_7L + 19V_8L \right\} \quad (13)$$

In Equation (13), the external loads are collected in the numerator while the measurements (w_5, w_9) are collected in the denominator. The estimation of EI_2 depends on the loading case and the measured displacements, not related to EI_1 or EI_3. Assume that L = 3 m, and the depth and width of the cross section are 0.5 m and 0.3 m. The inertia and the elastic modulus are 3.125×10^{-3} m^4 and 3.5×10^7 kN/m^2, respectively. A vertical concentrated load V_5 = 100 kN is applied at the one-third point. The ratio of the maximum deflection to the span is 1/760. The increments in the measured displacements obtained from FEM are listed in Table 1. Since V_5 = -100 kN and all the other loads are null, Equation (13) can be simplified as Equation (14).

$$EI_2^{set3} = \frac{V_5L^2}{2(w_5 - w_9)} = \frac{1}{\frac{2(w_5 - w_9)}{V_5L^2}} \quad (14)$$

Table 1. Increments in displacements for example 1 due to the concentrated load $V_5 = -100$ kN.

Displacements	Values	Unit
v_5	-0.010971	m
v_7	-0.011829	m
v_9	-0.009600	m
w_5	-0.001829	rad
w_9	0.002286	rad

As can be observed in Equation (14), the analytical equation of stiffnesses includes the term $w_5 - w_9$. Hence, the sign of the analytical equation can be affected by the sign of the term $w_5 - w_9$. When errors are introduced into the measurements, the sign of the term $w_5 - w_9$ might be reversed. Consequently, negative *EI* values might appear. The advantage of this analytical method is that if such values appear, it is easy to locate the source of error and either to discard the results, to improve the measurement data or to change the measurement points to avoid close-to-zero values.

With Table 1, Equations (10)–(12), the distributions of $w_5 - w_9$ and $\frac{2(w_5 - w_9)}{V_5 L^2}$ as well as EI_2^{set3} can be obtained. The distributions for $EI_2^{set1}(v_5, v_7$ and $v_9)$ and $EI_2^{set2}(v_5, v_7$ and $w_9)$ were obtained in the same way. To validate the statistical analysis, 2000 samples of measurement set (v_5, v_7 and v_9) were generated by Equation (10) with an error level of 5%. Two thousand estimations of EI_2 were obtained. All estimations were normalized by their nominal values. The probability density curve of the estimation of EI_2 was obtained from the 2000 estimations using kernel density estimation, which was carried out by the ksdensity command in Matlab.

The validity of the proposed statistical analysis is justified by the complete agreement between the estimated probability density curve and the theoretical one from Equation (11) in Figure 4a. The distribution of EI_2 using set 1 (v_5, v_7 and v_9) is severely right skewed, characterized by the extremely long right tail. At low error levels, the positive mode occurs close to one and the value of probability density is high for all three sets. This is no longer true as error levels increase. Figure 4b,c provide the probability density curves for the estimations of EI_2 using set 1 and set 3 with 20% error. For set 1, the biased positive mode x = 0.535 is related to a small density of 0.971. In addition, the negative mode x = −1.152 is not negligible. On the contrary, for set 3, the positive mode x = 0.990 is related to a much higher probability density of 5.664, while the negative mode x = −99.771 is negligible and hence not shown. This implies that for high error levels, the estimation using deflections leads to underestimations, and even negative estimations. In addition, the severe right skewness of the probability density curve for set 1 indicates a much larger variation in the estimations than in the case of using rotations (set 3).
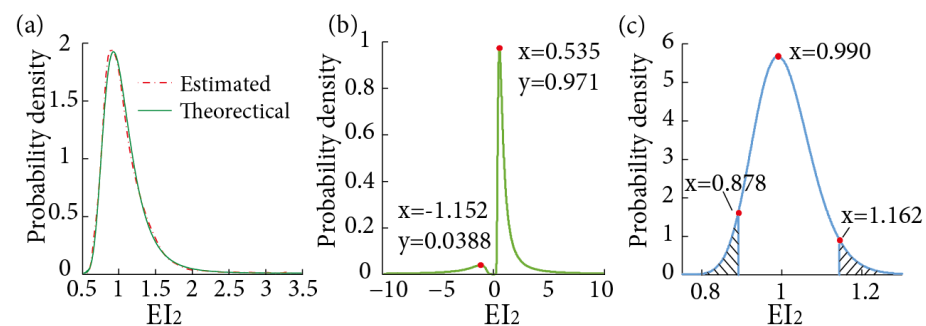

Figure 4. Probability density curves for the estimations of EI_2 using (**a**) set 1 (v_5, v_7 and v_9) with 5% error (theoretical distribution and inferred from data), (**b**) set 1 (v_5, v_7 and v_9) with 20% measurement error and (**c**) set 3 (w_5, w_9) with 20% measurement error (shaded area for 2.5% and 97.5% percentiles). (KDE for kernel density estimation).

The 95% confidence intervals of the estimations of EI_2 using set 3 with error levels ranging from 0% to 20% are depicted in Figure 5. The lower and upper bounds of the confidence interval are the cutting points of the 2.5% regions on the left and right sides of the probability density curve (shaded in Figure 4c). Figure 5 shows that the bounds of these confidence intervals satisfy a linear relation with the error level. In addition, these intervals are bounded by $[1 - E_{level}, 1 + E_{level}]$ for each error level.
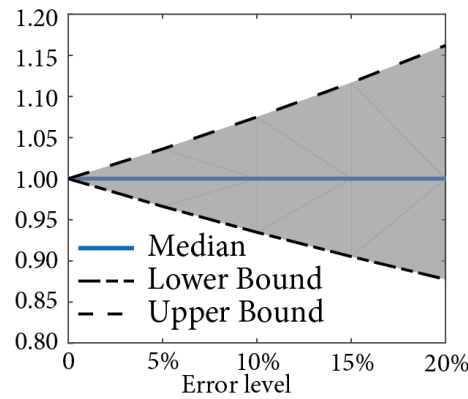

Figure 5. Confidence interval of the estimation for EI_2 under different error levels.

Figure 6 provides the variations inj the positive mode, the mean and the coefficient of variation (c.o.v.) for the estimations of EI_2 using different sets at different error levels. The median is always one for set 3 at any error level. The mean and the c.o.v. were analyzed with the interval [0, 2]. The remarkable consistency between the mode and the mean for set 3 justifies the unbiasedness of the estimations using rotations (Figure 6a). With 20% error, the deviation in the mean is 0.24% and the related c.o.v. is 0.046. On the contrary, the deviations in the mean increase rapidly with errors for set 1 and set 2. The positive mode for set 1 was close to zero when the error level was high. This indicates a large c.o.v., as seen in Figure 6b, and a right skewness. When more deflections were used, larger c.o.v.s were observed as the positions of the c.o.v. curves became higher.
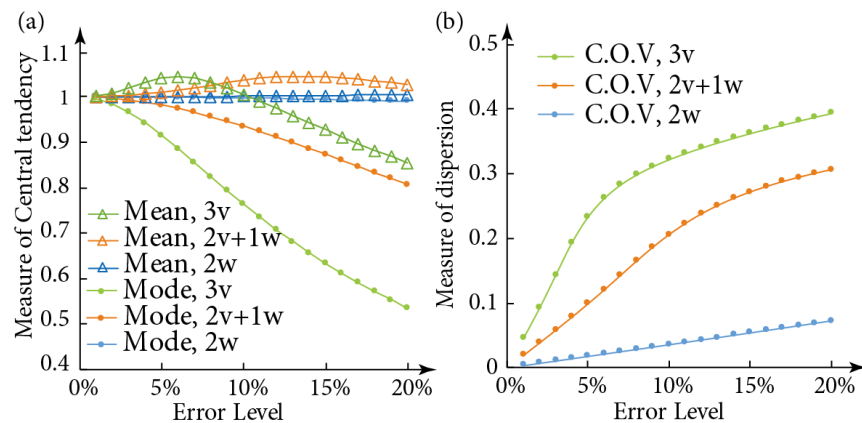

Figure 6. For the estimations of EI_2 using different sets ($3v$ for (v_5, v_7 and v_9), $2v + 1w$ for (v_5, v_7, w_9), $2w$ for (w_5 and w_9)) under error levels of 1~20%: (**a**) mean and mode, (**b**) coefficient of variation (c.o.v.).

This analysis shows that: (1) The statistical analysis is capable of analyzing the distribution of the estimations. (2) When the error level is high, the estimations using deflections might be negative and the distribution is severely right skewed. (3) Unlike the case of using deflections, the estimations using rotations are robust and insensitive to error levels, since the confidence intervals of the estimations are well bounded. (4) The higher the number of deflections used in the measurements, the higher the sensitivity of the estimations to errors.

This is because the measurements appear in the denominator of the analytical solution of stiffnesses. As demonstrated before, the value of the stiffness EI_2 is affected by the values of the term $w_5 - w_9$. When measurement errors are considered and $w_5 - w_9$ is close to zero, the value of EI_2 will vary drastically. When more deflections are used, the denominator of the corresponding stiffnesses is also composed of terms such as $w_i - v_j/L + v_k/L$. The denominator in the analytical solution of stiffnesses using more deflections is more sensitive to error. This is because the order of magnitude for the values of deflections is normally higher than that of rotations. The value of the denominator for measurement sets using deflections is much easier to be a close-to-zero value than the case of using rotations. As a result, the resulting estimation using more deflections seems to be more disperse.

3.2. Statistical Analysis of a Two-Story One-Bay Frame

To further verify the proposed method, statistical analysis was carried out for a two-story one-bay frame. The elastic modulus was 3.5×10^7 kN/m². The area and inertia of the columns were 0.24 m² and 7.2×10^{-3} m⁴, while the area and inertias of the beams were 0.15 m² and 3.125×10^{-3} m⁴. The parameterization of the FEM for this structure is shown in Figure 7a. A uniform load of 45 kN/m was applied to the second story. The bending stiffness EI_9 in the middle part of this story was the target parameter. To identify EI_9, four rotations or five deflections were required. Without loss of generality, two sets were used for structural system identification. Set 1 comprised four rotations (green) and set 2 comprised five deflections (red) (see Figure 7a). As the analytical expression for EI_9 is not concise, it is not provided here. The probability density curves for the estimations of EI_9 for these sets under different error levels (indicated in the brackets) are presented in Figure 7b. For set 1 (dashed lines), the positive modes always center around 1 and the negative ones are negligible. As the errors increase, the probability density curve for the estimation of EI_9 using rotations becomes wider and flatter. At the error level of 5%, the mean and the positive mode are 1.025 and 0.957, respectively. However, the estimations using deflections (solid lines) are very sensitive to error levels. The bimodality of the distribution for EI_9 is observed with a minor error of 0.2%. In addition, the positive modes are greatly deviated from 1. The positive modes related to 0.2% error and 1% error are 0.695 and 0.222, respectively.
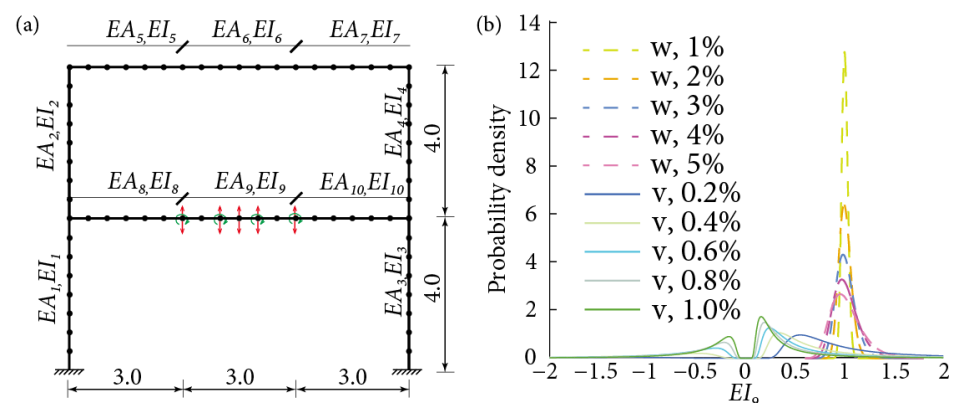

Figure 7. (**a**) FEM for a two-story one-bay frame (arrows denote deflections, arcs denote rotations). (**b**) The distributions of the estimations using rotations (*w*) or deflections (*v*) under different error levels (indicated in the brackets).

This analysis shows that: (1) the estimations using deflections are extremely sensitive to measurement errors in frame structures. (2) Measuring rotations outperforms measuring deflections regarding both the unbiasedness and the extent of variation in the estimations of the target parameter. It should also be pointed out that in frames, measuring rotations might be more practical since finding a reference point to measure deflections is non-trivial.

4. Using Redundant Rotations for Parameter Estimation

When essential measurement sets are used, the target parameters are observable. However, due to the ill-conditioned inverse problem, the estimations using essential sets are far from satisfactory. A reasonable solution to alleviate the adverse effect of measurement errors is to include redundant measurements. Four strategies to use redundant rotations are presented in Section 4.1. The effectiveness of these strategies was investigated in two structures regarding the estimation accuracy and dispersion. The first structure (Section 4.2) was a simply supported bridge (Figure 3) and the second (Section 4.3) was a 13-story frame structure.

4.1. Strategies to Use Redundant Measurements

In the case of redundant measurements with errors, the observability equations cannot be satisfied strictly. Numerical estimations were obtained by using the least squares method. However, the redundant measurement can be divided into several essential sets. For each essential set, a unique solution can be obtained. Hence, four strategies to use redundant rotations are presented as follows.

Strategy 1: Formulate the observability equations (Equation (6)) employing structural system identification using COM with all rotations in one batch. In this case, the equations cannot be satisfied strictly as measurement errors exist and the equations are solved directly using the least squares method.

Strategy 2: Derive the geometrical relations (referred to as compatibility conditions) that the nodal displacements should satisfy first [25]. Impose these compatibility conditions using optimization techniques by minimizing the discrepancy between the measured shape and the compatible one. The estimations of the parameters are obtained by providing the compatible displacements in Equation (6).

Strategy 3: The estimations using the redundant measurement sets are obtained in several batches. In each batch, the target parameters are obtained using one essential set, which is a subset of the redundant set. The final estimations are the average of the estimations from all batches. This strategy is also noted as an averaging method.

Strategy 4: The averaging method is carried out first. Then, the outliers in the estimations from different batches are detected and removed. The final estimations are the average of the remaining valid estimations. To determine outliers, the first quantile Q_1 and the third quantile Q_3 of the estimations from different batches are calculated. By the assumption of normal distribution, valid estimations should fall into the interval $[Q_1 - 2.7(Q_3 - Q_1), Q_3 + 2.7(Q_3 - Q_1)]$ with a coverage of 99.7%. Hence, values outside of this range are invalid and ruled out.

4.2. Verification for a Simply Supported Bridge

These four strategies were applied to the simply supported bridge described in Section 3.1 (Figure 3). Investigations of the estimations of parameters of a local zone and of the whole structure are presented in Sections 4.2.1 and 4.2.2.

4.2.1. Case 1: Parameter Estimation for a Local Region

The load case was the same as the one in Section 3.1. The target parameter was EI_2 and five rotations (w_5–w_9) were measured; 200 samples were generated for both error levels of 5% and 10%, and 200 estimations were carried out for each error level; $10 (= C_5^2)$ essential sets were able to identify EI_2 as two rotations were sufficient to identify EI_2. In strategy 3, the final estimation was the average of the 10 estimations from these sets. The boxplots of the estimations using the four strategies and the respective essential sets are depicted in Figure 8. The first four columns are the results for the proposed strategies while the last 10 columns are the results for respective essential sets. Great bias in the mean and a large variation are seen for estimations obtained using strategy 1. This is due to the formation of the observability equation. It is noted that the values of the rotations are mainly fed into the coefficient matrix. Additionally, the solutions of the equations are very

sensitive to the values of the entries in the coefficient matrix. When strategy 1 is used, the solution is obtained using the least squares method. In such cases, the solution obtained from an ill-posed coefficient matrix may be quite far from reasonable values. Hence, this strategy is no longer investigated in the subsequent studies. In the case of strategies 2–4, the estimations are unbiased and robust.
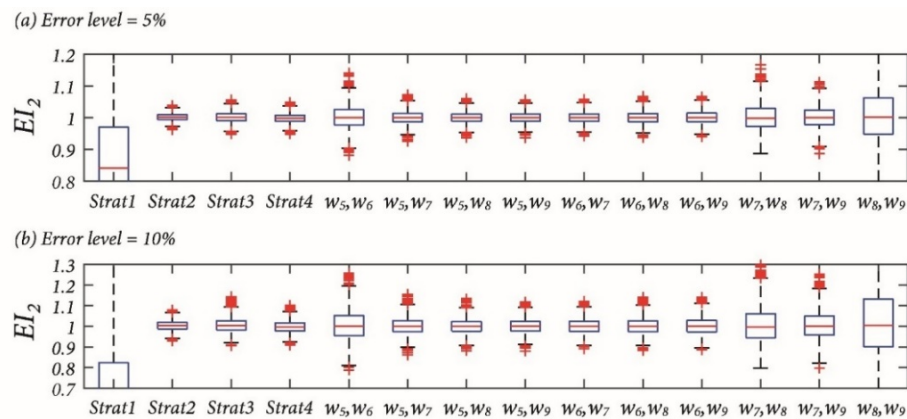

Figure 8. Box plot of the estimations of the bending stiffness EI_2 using different strategies and essential sets with (**a**) error level = 5%; (**b**) error level = 10%. (Strat abbreviated for strategy.)

Regarding the dispersion in the estimations, the best result was observed in the case of imposing compatibility conditions (strategy 2). The extents of dispersion corresponding to strategies 3 and 4 were also well controlled. After the outliers were ruled out, the c.o.v. of the estimations decreased from 0.016 (strategy 3) to 0.014 (strategy 4) at the error level of 5%. A decrease from 0.034 to 0.028 was also observed at the error level of 10%. The distributions of the estimations using strategies 2–4 at error levels of 5% and 10% are depicted by the probability density curves in Figure 9. It is seen that the deviations in the estimations are bounded by the error levels.
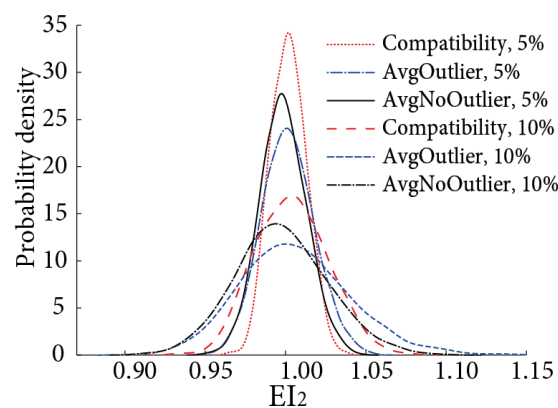

Figure 9. The probability density curve of the estimations using strategies 2 (compatibility conditions), 3 (averaging) and 4 (averaging with outliers ruled out).

4.2.2. Case 2: Parameter Estimation for the Whole Structure

In this section, the target parameters are the three bending stiffnesses EI_1–EI_3. Two load cases were studied. In the load case 1 (Figure 10a), a concentrated load $V_5 = 100$ kN was applied at one-third point (node 5) of the structure, while in load case two (Figure 10b), a uniformly distributed load $q = 20$ kN/m was applied over the whole span.

For both load cases, seven rotations were measured and their locations are indicated in Figure 10a,b. According to the observability analysis, there were 32 essential measurement sets able to identify the parameters of this structure. Hence, the estimations of the bending stiffnesses for strategies 3 and 4 were calculated by averaging the estimations from these

32 essential sets. To check the performance of different strategies, 200 measurement sets were generated using Equation (10). The 200 estimations for EI_1–EI_3 using strategies 2–4 are illustrated as the nine columns of boxplots in Figure 10c,d. The corresponding mean and c.o.v.s are presented in Table 2.
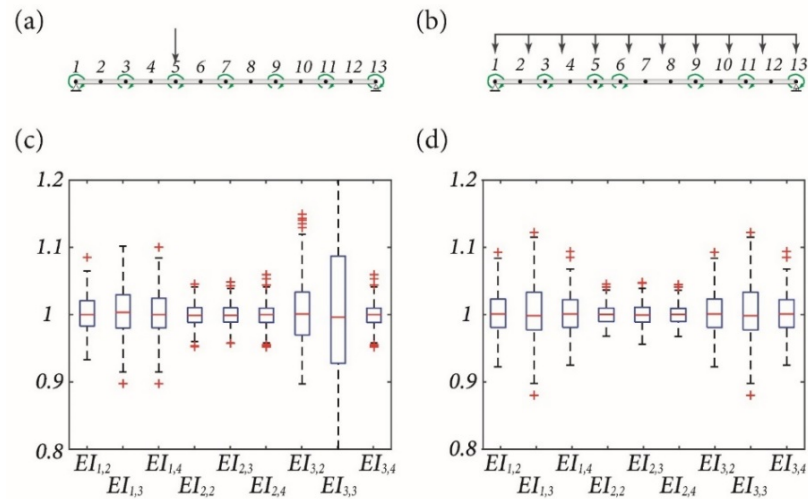

Figure 10. (**a**) Load case 1 (a concentrated load on the one-third point) and the measurement location; (**b**) load case 2 (a uniform load over the span) and the measurement location; (**c**) boxplots of the estimations under load case 1; (**d**) boxplots of the estimations using under load case 2 (note: $EI_{i,j}$ means the estimation of EI_i using strategy j).

The parameters and strategies are indicated by the subscripts of the x labels in these figures. For instance, $EI_{2,3}$ denotes the estimation of the bending stiffness EI_2 using strategy 3. As observed in Table 2 and Figure 10c, all the estimations from different strategies were unbiased as the mean was always located at 1. Regarding the c.o.v., imposing the compatibility condition (strategy 2) achieved the best performance for all parameters in both load cases 1 and 2. The extent of dispersion in the estimations was significant for those obtained from strategy 3. After strategy 4 was adopted, the c.o.v.s for estimations using strategy 3 reduced as outliers were ruled out. A decrease in c.o.v.s for EI_3 in load case 1 from 0.123 to 0.055 was observed. From the result for load case 2, similar conclusions can be drawn. In addition, the performance of using strategy 4 was very close to that of using strategy 2. The comparison between the results from load cases 1 and 2 shows the effect of load case on the estimation accuracy. The poor estimation in EI_3 is due to the less excited flexural behavior of this region in load case 1. In load case 2, the mid span region was well excited and the zones adjacent to the supports were less excited under the external loads. Hence, the dispersion of the estimations for EI_2 was low while that for EI_1 and EI_2 was larger.

Table 2. Statistical summary of the estimations using different strategies.

Parameter	Load Case 1		Load Case 2	
	Mean	c.o.v.	Mean	c.o.v.
$EI_{1,2}$	1.001	0.027	1.001	0.030
$EI_{1,3}$	1.003	0.038	1.003	0.043
$EI_{1,4}$	1.002	0.035	1.002	0.031
$EI_{2,2}$	1.000	0.017	1.000	0.014
$EI_{2,3}$	1.000	0.018	1.001	0.017
$EI_{3,4}$	1.000	0.017	1.000	0.014
$EI_{3,2}$	1.003	0.050	1.001	0.030
$EI_{3,3}$	1.014	0.123	1.003	0.043
$EI_{3,4}$	1.002	0.055	1.002	0.031

From this section, it is concluded that in the bridge example: (1) Incorporating all redundant measurements in the observability equation in one batch leads to greatly biased estimations; this can be tackled by proposed strategies 2–4. (2) Imposing compatibility conditions (strategy 2) is the best strategy regarding the unbiasedness and dispersion of the estimations. (3) Averaging the estimations from different essential sets also leads to satisfactory estimations. The result can be further improved by ruling out the outliers in the estimations using different essential sets.

4.3. Verification for a High-Rise Frame Structure

Strategy 2 cannot be applied in frame structures as the compatibility condition is not available in such structures. Hence, strategy 4 was applied in the identification of parameters of a frame structure simulated by a FEM [49] studied previously (see Figure 11a). In that study, the observability of the parameters was studied symbolically, while the numerical analysis and the effect of measurement errors were not included. In this paper, the focus is the identification of the bending stiffness of the floor slab in the middle right of the third floor. Figure 11b shows the FEM for this part. It is parameterized by three bending stiffnesses, EI_9–EI_{11}. The parameterization of the remaining part is the same as that in [49]. The bending stiffnesses $EI_9 = EI_{10} = 1.75 \times 10^8$ N m^2. Damage to the right side of the target floor slab was simulated by a 30% reduction in bending stiffness EI_{11}, i.e., $EI_{11} = 1.225 \times 10^8$ N·m^2. An overload of 40 kN/m was applied to this floor slab to simulate a static load test. Due to the unsatisfactory result of using deflections, 10 rotations ($w_{32}, w_{72}, w_{74}, w_{76}, w_{78}, w_{80}, w_{82}, w_{84}, w_{86}$ and w_{46}) were measured to identify EI_9–EI_{11}. The increments in the rotations due to this load were calculated by direct analysis. Five error levels (1–5%) were studied. For each error level, 100 measurement sets were generated using Equation (10). To identify EI_9–EI_{11}, two rotations were required for each parameter. Taking two rotations from ($w_{32}, w_{72}, w_{74}, w_{76}$), ($w_{76}, w_{78}, w_{80}, w_{82}$) and ($w_{82}, w_{84}, w_{86}, w_{46}$), respectively, EI_9–EI_{11} led to 117 essential sets composed of six rotations. Thus, 117 estimations were obtained for each measurement set and the outliers in these estimations were ruled out. Figure 11c presents the error bar of the final estimations of EI_9–EI_{11} under different error levels. The centerlines indicate the mean of estimations for each set. The vertical error bars cover two standard deviations of the estimations. Hence, the length of these bars indicates the extent of dispersion in the estimations.
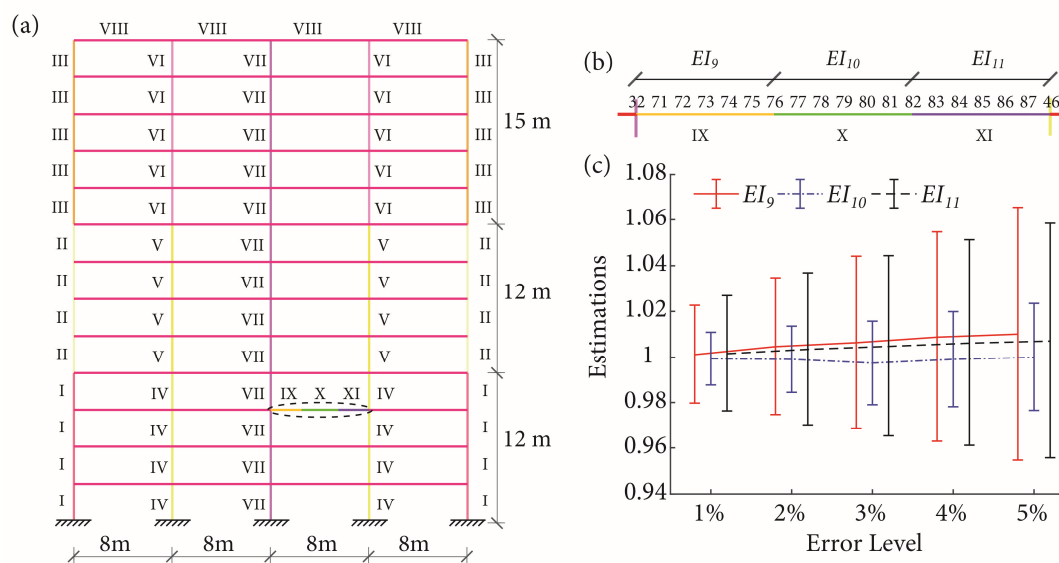

Figure 11. (**a**) The FEM of the high-rise building (adapted from [49]). (**b**) The FEM for the floor slab to be identified. (**c**) Error bar plot of the estimations of EI_9–EI_{11}.

From Figure 11, it is seen that: (1) The estimations are unbiased, since the centerline is located at 1. (2) The estimations of EI_{10} always have the least variation. (3) The increase in variations in the estimations follows a linear relationship with error levels. (4) The sensitivity of the increase of variation with error levels is the lowest for EI_{10}. In fact, the better estimations in EI_{10} are due to the higher curvature of the zones parameterized by EI_{10} than the remaining zones, which agrees with the result in the previous study [24].

In the current study, only rotations were used in the measurement sets. The possibility of using the combination of deflections and rotations will be investigated in future study.

5. Conclusions

This article proposes a statistical analysis to illustrate the theoretical advantage of measuring rotations rather than deflections in static structural system identification, which is also different from the system identification using dynamic data [50–52]. With this aim, the analytical expressions for the target parameters are derived with structural system identification using the constrained observability method. Combining these expressions and the inverse distribution theory, a procedure for obtaining the distributions of the estimations is proposed for the very first time. The statistical analyses were carried out in two structures. Its effectiveness was verified by comparison with a Monte Carlo analysis. From the numerical examples, the distributions of the estimations using only deflection measurements are very sensitive to errors. These distributions explain the reason for the biased or even negative estimations when only deflections are measured in the case of essential sets. In the comparative study of measuring deflections or rotations, it is justified that the estimations using rotations are always less sensitive to measurement errors than those using deflections, with respect to the unbiasedness and the extent of variation in the estimations.

Taking account of the theoretical and practical advantages of using rotations, four strategies for using redundant rotations to improve the accuracy of estimations were proposed and compared in different structures under static loading. In the simply supported bridge example where the compatibility conditions were obtainable, the strategy of using compatibility conditions outperformed the rest. The performance of strategy 4 (averaging with outliers ruled out) was entirely satisfactory. Furthermore, strategy 4 can be applied in frame structures where the compatibility conditions are not available. In the numerical analysis of the high-rise frame, the satisfactory accuracy and robust performance achieved by using rotations along with strategy 4 justify the effectiveness and versatility of the proposed method. The theoretical basis of this method has been established in this paper and it has been proved that with numerically generated data the method is able to provide sensible results and improve the predictions obtained with just deflections. However, empirical validation is lacking, and this has to be checked to confirm that the practical application of the method is feasible. Moreover, applications based on field measurement will also be carried out in future work.

Conflicts of Interest: The authors declare no conflict of interest.

Nomenclature

$[A]$	A $m \times n$ matrix	$\{z\}$	Unknown vector
$[N]$	Null space matrix	$\{z_g\}$	General solution vector
$[K]$	Global stiffness matrix	$\{z_p\}$	Particular solution vector
L	Length	$\{z_h\}$	One solution vector to the homogeneous equation
E	Elastic moduli	$\{D\}$	Constant vector
A	Area	$\{\rho\}$	Coefficient vector
I	Inertia	$\{z_s\}$	Single variables vector
$\{\delta\}$	Displacement vector	$\{z^*\}$	A new unknown vector by adding $\{z_s\}$ in $\{z\}$
U	Horizontal deflection	$[\Omega]$	A null matrix
V	Vertical deflection	$[B^*]$	A new coefficient matrix by introducing null matrix $[\Omega]$
W	Rotation	ϵ	Residual
$\{f\}$	Force vector	$\tilde{\delta}$	Random errors
H	Horizontal force	δ_r	Displacement obtained from FEM
V	Vertical force	E_{level}	Error level
M	Moment	ζ	Random number follows a normal distribution with zero mean and standard deviation 0.5
N_e	Number of elements	μ	Mean value
N_n	Number of nodes	σ	Standard deviation
$[K^*]$	Modified global stiffness matrix	X	Random variable
$\{\delta^*\}$	Modified displacement vector	Y	The inverse distribution of X
I	Identity matrices	p_Y	Probability density function of Y
0	Null matrices	θ	Target parameter
$[B]$	Coefficient matrix	D_{denom}	Reciprocal of target parameter θ

References

1. Al-Hussein, A.; Haldar, A. Structural damage prognosis of three-dimensional large structural systems. *Struct. Infrastruct. Eng.* **2017**, *13*, 1596–1608. [CrossRef]
2. Davoudi, R.; Miller, G.R.; Kutz, J.N. Data-driven vision-based inspection for reinforced concrete beams and slabs: Quantitative damage and load estimation. *Autom. Constr.* **2018**, *96*, 292–309. [CrossRef]
3. Morgenthal, G.; Hallermann, N.; Kersten, J.; Taraben, J.; Debus, P.; Helmrich, M.; Rodehorst, V. Framework for automated UAS-based structural condition assessment of bridges. *Autom. Constr.* **2019**, *97*, 77–95. [CrossRef]
4. Deraemaeker, A.; Ladevèze, P.; Leconte, P. Reduced bases for model updating in structural dynamics based on constitutive relation error. *Comput. Methods Appl. Mech. Eng.* **2002**, *191*, 2427–2444. [CrossRef]
5. Christodoulou, K.; Ntotsios, E.; Papadimitriou, C.; Panetsos, P. Structural model updating and prediction variability using Pareto optimal models. *Comput. Methods Appl. Mech. Eng.* **2008**, *198*, 138–149. [CrossRef]
6. Jensen, H.E.; Millas, E.; Kusanovic, D.; Papadimitriou, C. Model-reduction techniques for Bayesian finite element model updating using dynamic response data. *Comput. Methods Appl. Mech. Eng.* **2014**, *279*, 301–332. [CrossRef]
7. Park, H.S.; Oh, B.K. Real-time structural health monitoring of a supertall building under construction based on visual modal identification strategy. *Autom. Constr.* **2018**, *85*, 273–289. [CrossRef]
8. Beck, J.L.; Katafygiotis, L.S. Updating models and their uncertainties. I: Bayesian statistical framework. *J. Eng. Mech.* **1998**, *124*, 455–461. [CrossRef]
9. Papadimitriou, C.; Lombaert, G. The effect of prediction error correlation on optimal sensor placement in structural dynamics. *Mech. Syst. Signal Process.* **2012**, *28*, 105–127. [CrossRef]
10. Goulet, J.-A.; Smith, I.F.C. Structural identification with systematic errors and unknown uncertainty dependencies. *Comput. Struct.* **2013**, *128*, 251–258. [CrossRef]

11. Proverbio, M.; Vernay, D.G.; Smith, I.F.C. Population-based structural identification for reserve-capacity assessment of existing bridges. *J. Civ. Struct. Health Monit.* **2018**, *8*, 363–382. [CrossRef]

12. Alvin, K. Finite element model update via Bayesian estimation and minimization of dynamic residuals. *AIAA J.* **1997**, *35*, 879–886. [CrossRef]

13. Sanayei, M.; Scampoli, S.F. Structural Element Stiffness Identification from Static Test Data. *J. Eng. Mech.* **1991**, *117*, 1021–1036. [CrossRef]

14. Banan, M.; Hjelmstad, K.D. Parameter Estimation of Structures from Static Response. I. Computational Aspects. *J. Struct. Eng.* **1994**, *120*, 3243–3258. [CrossRef]

15. Hjelmstad, K.D.; Shin, S. Damage Detection and Assessment of Structures from Static Response. *J. Eng. Mech.* **1997**, *123*, 568–576. [CrossRef]

16. Yang, Q.; Sun, B. Structural damage localization and quantification using static test data. *Struct. Health Monit.* **2010**, *10*, 381–389. [CrossRef]

17. Sun, Z.; Nagayama, T.; Fujino, Y. Minimizing noise effect in curvature-based damage detection. *J. Civ. Struct. Health Monit.* **2016**, *6*, 255–264. [CrossRef]

18. Castillo, E.; Conejo, A.J.; Pruneda, R.E.; Solares, C. Observability in linear systems of equations and inequalities: Applications. *Comput. Oper. Res.* **2007**, *34*, 1708–1720. [CrossRef]

19. Castillo, E.; Conejo, A.; Pruneda, R.; Solares, C. Observability Analysis in State Estimation: A Unified Numerical Approach. *IEEE Trans. Power Syst.* **2006**, *21*, 877–886. [CrossRef]

20. Castillo, E.; Lozano-Galant, J.A.; Nogal, M.; Turmo, J. New tool to help decision making in civil engineering. *J. Civ. Eng. Manag.* **2015**, *21*, 689–697. [CrossRef]

21. Nogal, M.; Lozano-Galant, J.A.; Turmo, J.; Castillo, E. Numerical damage identification of structures by observability techniques based on static loading tests. *Struct. Infrastruct. Eng.* **2015**, *12*, 1216–1227. [CrossRef]

22. Tomàs, D.; Lozano-Galant, J.A.; Ramos, G.; Turmo, J. Structural system identification of thin web bridges by observability techniques considering shear deformation. *Thin-Walled Struct.* **2018**, *123*, 282–293. [CrossRef]

23. Emadi, S.; Lozano-Galant, J.A.; Xia, Y.; Ramos, G.; Turmo, J. Structural system identification including shear de-formation of composite bridges from vertical deflections. *Steel Compos. Struct.* **2019**, *32*, 731–741.

24. Lei, J.; Lozano-Galant, J.A.; Nogal, M.; Xu, D.; Turmo, J. Analysis of measurement and simulation errors in structural system identification by observability techniques. *Struct. Control Health Monit.* **2017**, *24*, e1923. [CrossRef]

25. Lei, J.; Xu, D.; Turmo, J. Static structural system identification for beam-like structures using compatibility conditions. *Struct. Control Health Monit.* **2017**, *25*, e2062. [CrossRef]

26. Lei, J.; Lozano-Galant, J.A.; Xu, D.; Turmo, J. Structural system identification by measurement error-minimizing observability method. *Struct. Control Health Monit.* **2019**, *26*, e2425. [CrossRef]

27. Chen, Z.W.; Cai, Q.L.; Zhu, S.; Wei, Z.; Qin, C.; Cai, L.; Zhu, S. Damage quantification of beam structures using deflection influence lines. *Struct. Control Health Monit.* **2018**, *25*, e2242. [CrossRef]

28. Ha, D.W.; Park, H.S.; Choi, S.W.; Kim, Y. A Wireless MEMS-Based Inclinometer Sensor Node for Structural Health Monitoring. *Sensors* **2013**, *13*, 16090–16104. [CrossRef]

29. Shang, Z.; Shen, Z. Multi-point vibration measurement and mode magnification of civil structures using video-based motion processing. *Autom. Constr.* **2018**, *93*, 231–240. [CrossRef]

30. Feng, M.Q.; Feng, S.; Beskhyroun, L.D.; Wegner, B.F.; Sparling, D.; Feng, M.Q. Vision-based multipoint displacement measurement for structural health monitoring. *Struct. Control Health Monit.* **2016**, *23*, 876–890. [CrossRef]

31. Lee, J.-J.; Ho, H.-N. A Vision-Based Dynamic Rotational Angle Measurement System for Large Civil Structures. *Sensors* **2012**, *12*, 7326–7336. [CrossRef]

32. Robert-Nicoud, Y.; Raphael, B.; Burdet, O.; Smith, I.F.C. Model Identification of Bridges Using Measurement Data. *Comput. Civ. Infrastruct. Eng.* **2005**, *20*, 118–131. [CrossRef]

33. Zhang, W.; Sun, L.M.; Sun, P.S.W. Bridge-Deflection Estimation through Inclinometer Data Considering Structural Damages. *J. Bridg. Eng.* **2017**, *22*, 04016117. [CrossRef]

34. Park, H.S.; Shin, Y.; Choi, S.W.; Kim, Y. An Integrative Structural Health Monitoring System for the Local/Global Responses of a Large-Scale Irregular Building under Construction. *Sensors* **2013**, *13*, 9085–9103. [CrossRef] [PubMed]

35. Liu, T.; Yang, B.; Zhang, Q. Health Monitoring System Developed for Tianjin 117 High-Rise Building. *J. Aerosp. Eng.* **2017**, *30*, B4016004. [CrossRef]

36. Kim, T.; Lim, H.; Kim, S.W.; Cho, H.; Kang, K.-I. Inclined construction hoist for efficient resource transportation in irregularly shaped tall buildings. *Autom. Constr.* **2016**, *62*, 124–132. [CrossRef]

37. Liu, D.; Wu, Y.; Li, S.; Sun, Y. A real-time monitoring system for lift-thickness control in highway construction. *Autom. Constr.* **2016**, *63*, 27–36. [CrossRef]

38. Ha, D.W.; Kim, J.M.; Kim, Y.; Park, H.S. Development and application of a wireless MEMS-based borehole inclinometer for automated measurement of ground movement. *Autom. Constr.* **2018**, *87*, 49–59. [CrossRef]

39. Dirksen, J.; Pothof, I.; Langeveld, J.; Clemens, F. Slope profile measurement of sewer inverts. *Autom. Constr.* **2014**, *37*, 122–130. [CrossRef]

40.   He, X.; Yang, X.; Zhao, L. New Method for High-Speed Railway Bridge Dynamic Deflection Measurement. *J. Bridge Eng.* **2014**, *19*, 05014004. [CrossRef]

41.   Hou, S.; Zeng, C.; Zhang, H.; Ou, J. Monitoring interstory drift in buildings under seismic loading using MEMS inclinometers. *Constr. Build. Mater.* **2018**, *185*, 453–467. [CrossRef]

42.   Bertola, N.J.; Papadopoulou, M.; Vernay, D.; Smith, I.F.C. Optimal multi-type sensor placement for structural identification by static-load testing. *Sensors* **2017**, *17*, 2904. [CrossRef] [PubMed]

43.   Papadimitriou, C. Optimal sensor placement methodology for parametric identification of structural systems. *J. Sound Vib.* **2004**, *278*, 923–947. [CrossRef]

44.   Argyris, C.; Papadimitriou, C.; Panetsos, P. Bayesian optimal sensor placement for modal identification of civil infra-structures. *J. Smart Cities* **2017**, *2*, 69–86. [CrossRef]

45.   Johnson, N.L.; Kotz, S.; Balakrishnan, N. *Continuous Univariate Distributions*, 2nd ed.; Wiley: Hoboken, NJ, USA, 1994.

46.   Lei, J.; Nogal, M.; Lozano-Galant, J.A.; Xu, D.; Turmo, J. Constrained observability method in static structural system identification. *Struct. Control Health Monit.* **2018**, *25*, e2040. [CrossRef]

47.   Abur, A.G. *Exposito, Power System State Estimation: Theory and Implementation*; CRC Press: Boca Raton, FL, USA, 2004.

48.   Lozano-Galant, J.A.; Nogal, M.; Turmo, J.; Castillo, E. Selection of measurement sets in static structural identification of bridges using observability trees. *Comput. Concr.* **2015**, *15*, 771–794. [CrossRef]

49.   Lozano-Galant, J.A.; Nogal, M.; Castillo, E.; Turmo, J. Application of observability techniques to structural system identification. *Comput.-Aided Civ. Infrastruct. Eng.* **2013**, *28*, 434–450. [CrossRef]

50.   Zhang, F.-L.; Au, S.-K.; Ni, Y.-C. Two-stage Bayesian system identification using Gaussian discrepancy model. *Struct. Health Monit. Int. J.* **2021**, *20*, 580–595. [CrossRef]

51.   Zhang, F.L.; Kim, C.W.; Goi, Y. Efficient Bayesian FFT method for damage detection using ambient vibration data with consideration of uncertainty. *Struct. Control Health Monit.* **2021**, *28*, e2659. [CrossRef]

52.   Ni, Y.C.; Zhang, F.L. Uncertainty quantification in fast Bayesian modal identification using forced vibration data considering the ambient effect. *Mech. Syst. Signal Process.* **2021**, *148*, 107078. [CrossRef]